

Vortex rings in fragmentation regions in heavy-ion collisions at $\sqrt{s_{NN}} = 39$ GeV

Yu. B. Ivanov^{1,2,3,*} and A. A. Soldatov²

¹*National Research Centre "Kurchatov Institute", Moscow 123182, Russia*

²*National Research Nuclear University "MEPhI", Moscow 115409, Russia*

³*Bogoliubov Laboratory of Theoretical Physics, JINR, Dubna 141980, Russia*

Vorticity generated in heavy-ion collisions at energy of $\sqrt{s_{NN}} = 39$ GeV is studied. Simulations are performed within a model of the three-fluid dynamics. A peculiar structure consisting of two vortex rings is found: one ring in the target fragmentation region and another one in the projectile fragmentation region. These rings are also formed in central collisions. The matter rotation is opposite in this two rings. These vortex rings are already formed at the early stage of the collision together with primordial fragmentation regions. The average vorticity, responsible for the global polarization of the observed Λ and $\bar{\Lambda}$, is also studied. In the semi-central collisions the average vorticity in the midrapidity region turns out to be more than an order of magnitude lower than the total one. The total vorticity is dominated by the contributions of the fragmentation regions and is produced because of asymmetry of the vortex rings in noncentral collisions. This suggests that in semi-central collisions the global polarization in the fragmentation regions should be at least an order of magnitude higher than that observed by the STAR collaboration in the midrapidity. This polarization should be asymmetrical in the reaction plane and correlate with the corresponding directed flow.

PACS numbers: 25.75.-q, 25.75.Nq, 24.10.Nz

Keywords: relativistic heavy-ion collisions, hydrodynamics, vorticity

I. INTRODUCTION

In peripheral collisions of high-energy heavy ions the system has a large angular momentum that results in observable consequences. In particular, it was proposed that Λ hyperons can be polarized along the angular momentum of two colliding nuclei [1–3]. Global polarization of Λ and $\bar{\Lambda}$ hyperons produced in heavy-ion collisions has been recently observed [4] by the STAR experiment in energy range of the Beam Energy Scan (BES) program at the Relativistic Heavy Ion Collider (RHIC) at Brookhaven. It was measured in the midrapidity region of colliding nuclei. It was concluded that the observed rotational fluid has the largest vorticity, of the order of $\sim 10^{22} \text{ s}^{-1}$, that ever existed in the universe. The measured polarization quantitatively agrees with the hydrodynamic [5, 6] and kinetic [7–10] model calculations.

However, important questions still remain: Why does the global polarization decrease with the collision energy rise as the total angular momentum increases? Where is the huge angular momentum mainly accumulated? These questions were indirectly answered in Refs. [11–13]. It was found that the vorticity, which is the driving force of the hadron polarization, is predominantly localized in a relatively thin layer at the boundary between participants and spectators. This implies that the hyperon polarization should be stronger at peripheral rapidities, corresponding to this border than in the midrapidity region. This enhancement at peripheral rapidities was illustrated in Ref. [8] at the example of Au+Au colli-

sion at $\sqrt{s_{NN}} = 5$ GeV. Although not all models predict the polarization minimum at the midrapidity [14]. The polarization enhancement at peripheral rapidities is not a direct explanation of the reduction of the midrapidity polarization with the collision energy rise but indicates that the hyperon polarization at peripheral rapidities may be very large as compared with that at the midrapidity in ultrarelativistic collisions and even higher than that at the lowest BEC-RHIC energy.

The study of the hyperon polarization at peripheral rapidities is not just of academic interest. Recent proposal [15] to perform experiments at the Large Hadron Collider (LHC) at CERN in the fixed-target mode revived interest to the fragmentation regions in relativistic nucleus-nucleus collisions. The LHC beam of lead ions interacting on a fixed target would provide an opportunity to carry out precision measurements in the kinematical range of the target fragmentation region. If the LHC operates in a fixed-target mode at the beam energy of 2.76 GeV per nucleon for lead nuclei, this is equivalent to $\sqrt{s_{NN}} = 72$ GeV in terms the center-of-mass energy.

In the present paper we analyze the vorticity in Au+Au collisions at the energy of $\sqrt{s_{NN}} = 39$ GeV. A special emphasis is made on the vorticity in the fragmentation regions. The vorticity is simulated within the model of the three-fluid dynamics (3FD) [16]. The 3FD model is quite successful in reproduction of the major part of bulk observables: the baryon stopping [17, 18], yields of different hadrons, their rapidity and transverse momentum distributions [19, 20], and also the elliptic [21] and directed [22] flow excitation functions. In recent paper [23] it was demonstrated that the 3FD model successfully reproduces the extensive set of bulk observables at midrapidity recently presented by the STAR Collaboration [24]. Therefore, the 3FD predictions for the frag-

*e-mail: Y.Ivanov@gsi.de

mentation regions may be of interest.

II. THE 3FD MODEL

The 3FD approximation is a minimal way to simulate the early-stage nonequilibrium in the colliding nuclei at high incident energies. In contrast to the conventional hydrodynamics, a finite stopping power resulting in a counterstreaming regime of leading baryon-rich matter at early stage of the nuclear collision is taken into account in the 3FD description [16]. This nonequilibrium state of the baryon-rich matter is modeled by two interpenetrating baryon-rich fluids initially associated with constituent nucleons of the projectile (p) and target (t) nuclei. At later stages these baryon-rich fluids may consist of any type of hadrons and/or partons (quarks and gluons), rather than only nucleons. Newly produced particles, which populate the midrapidity region, are associated with a fireball (f) fluid. Each of these fluids is governed by conventional hydrodynamic equations coupled by friction terms in the right-hand sides of the Euler equations. These friction terms describe energy-momentum loss of the baryon-rich fluids. A part of this loss is transformed into thermal excitation of these fluids, while another part gives rise to particle production into the fireball fluid.

The physical input of the present 3FD calculations is described in Ref. [17]. The friction between fluids was fitted for each EoS to reproduce the observed stopping power, see Ref. [17] for details. The simulations in [17–22] were performed with different equations of state (EoS's)—a purely hadronic EoS [25] and two versions of the EoS involving the deconfinement transition [26], i.e. a first-order phase transition and a smooth crossover one. In the present paper we demonstrate results with only the first-order-phase-transition (1st-order-tr.) and crossover EoS's as the most successful in reproduction of various observables, in particular, the recent data on bulk observables at $\sqrt{s_{NN}} = 39$ GeV [23].

In semi-central Au+Au collisions at the energy of $\sqrt{s_{NN}} = 39$ GeV the counterstreaming of leading baryon-rich matter takes place only during short initial stage. After a short time ≈ 1 fm/c the p- and t-fluids are either spatially separated or mutually stopped and unified, thus forming a unified single baryon-rich fluid similarly to that happening in central collisions at this energy [27]. Indeed, the corresponding unification measure

$$1 - \frac{n_p + n_t}{n_B} \quad (1)$$

at $t \gtrsim 1$ fm/c is less than 0.01. Here

$$n_B = |J_B| = (J_B^\mu J_{B\mu})^{1/2} \quad (2)$$

is the proper (i.e. in the local rest frame) baryon density of the unified baryon-rich fluid defined in terms of the baryon current $J_B^\mu = n_p u_p^\mu + n_t u_t^\mu$, where n_α and u_α^μ are the proper baryon densities and hydrodynamic

4-velocities of the p- and t-fluids, respectively. This unification measure is zero, when the p- and t-fluids are mutually stopped and unified, and has a positive value increasing with rise of the relative velocity of the p- and t-fluids.

The f-fluid also is entrained by the unified baryon-rich fluid but is not that well unified with the latter. The local baryon-fireball relative velocity is $v_{fB} \lesssim 0.2$, at $t \gtrsim 1$ fm/c, i.e. it is small but not negligible. In particular, the friction between the baryon-rich and net-baryon-free fluids is the only source of dissipation at the expansion stage. Thus, at $t \gtrsim 1$ fm/c the system is characterized by two hydrodynamical velocities, u_B^μ and u_f^μ , attributed to the baryon-rich and baryon-free fluids, respectively, and two corresponding temperatures T_B and T_f .

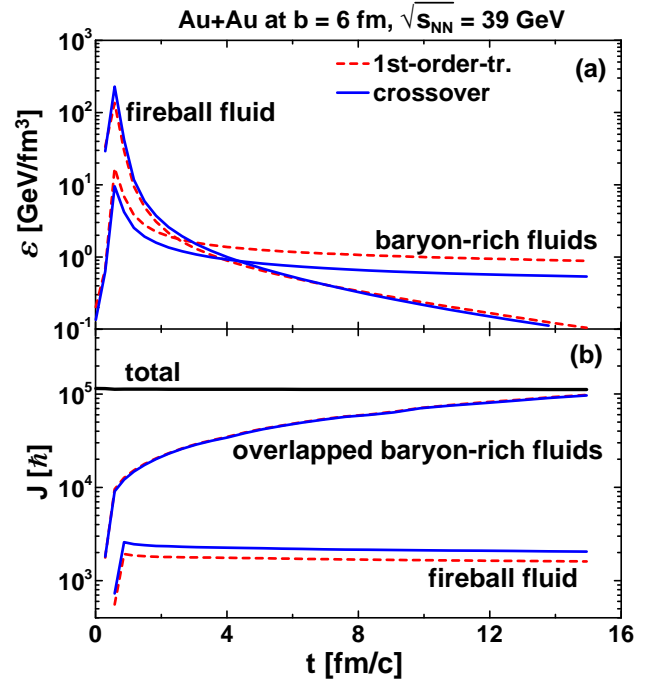


FIG. 1: (Color online) Time evolution of (a) average proper energy densities of the baryon-rich and baryon-free fluids and (b) the total angular momentum (conserved quantity), the angular momentum accumulated in the baryon-rich fluids in their overlap region and the angular momentum of the fireball fluid in the semi-central ($b = 6$ fm) Au+Au collision at $\sqrt{s_{NN}} = 39$ GeV. Calculations are done with the first-order-phase-transition and crossover EoS's.

In Fig. 1 the time evolution of average proper energy densities of the baryon-rich and baryon-free fluids [panel (a)] and the total angular momentum, the angular momentum of the baryon-rich fluids in their overlap region and the angular momentum of the fireball fluid [panel (b)] in the semi-central ($b = 6$ fm) Au+Au collision at $\sqrt{s_{NN}} = 39$ GeV are presented. As seen, at $t < 4$ fm/c the f-fluid dominates, i.e. its average energy density exceeds that of the baryon-rich fluid. Whereas at $t > 4$ fm/c, the situation is reversed – the baryon-rich fluid

dominates. As seen from Fig. 2 (baryon-density and energy-density columns), it dominates in fragmentation regions where the baryon charge is concentrated.

The total angular momentum (that includes a contribution of spectators) is a conserved quantity. It is determined as

$$J = \int d^3x \sum_{\alpha=p,t,f} (z T_{10}^\alpha - x T_{30}^\alpha). \quad (3)$$

where $T_{\mu\nu}^\alpha$ is the energy-momentum tensor of the $\alpha(=p,t,f)$ fluid that have the conventional hydrodynamical form, z is the beam axis, (x, z) is the reaction plane of the colliding nuclei. The constancy of the total angular momentum [Fig. 1, panel (b)] demonstrates the accuracy of the numeric scheme: J_{total} is conserved with the accuracy of 1%. The overlap region of the baryon-rich fluids rises in the course of the expansion stage and includes more and more former spectators. Thus, the angular momentum of the baryon-rich fluid in their overlap almost accumulates the major part of the total angular momentum of the system at the final stage of the collision, cf. Fig. 1, panel (b). The angular momentum of the newly produced f-fluid is almost two orders of magnitude lower than that of the overlapped baryon-rich fluids at the final stage of the collision.

III. VORTICITY IN THE 3FD MODEL

There are several definitions of the vorticity that are suitable for calculations of the hadron polarization in different approaches. In the present study we consider the relativistic kinematic vorticity

$$\omega_{\mu\nu} = \frac{1}{2}(\partial_\nu u_\mu - \partial_\mu u_\nu), \quad (4)$$

where u_μ is a collective local four-velocity of the matter. This type of the vorticity is directly relevant to the hadron polarization due to the chiral vortical effect [28] that was used in Refs. [7, 8]. Another type of the vorticity is so-called thermal vorticity

$$\varpi_{\mu\nu} = \frac{1}{2}(\partial_\nu \hat{\beta}_\mu - \partial_\mu \hat{\beta}_\nu), \quad (5)$$

where $\hat{\beta}_\mu = \hbar\beta_\mu$ and $\beta_\mu = u_\mu/T$ with T being the local temperature. Thus, ϖ is dimensionless. It is directly related to the polarization vector of a spin 1/2 particle in the thermodynamical approach [29] that was used in Refs. [5, 6, 9, 10].

As it was argued above, at $t \gtrsim 1$ fm/c the system is characterized by two hydrodynamical velocities, u_B^μ and u_f^μ , and two corresponding temperatures, T_B and T_f , corresponding to the unified baryon-rich fluid (B) and the baryon-free fluid (f). Thus we deal with two sets of the vorticity attributed to these baryon-rich and baryon-free fluids, respectively.

In order to suppress contributions of almost empty regions, where the matter is relatively thin, we consider a proper-energy-density weighted vorticity in the reaction (xz) plane, i.e. at $y = 0$, similarly to that done in Ref. [11]. Moreover, we sum the vorticity of the baryon-rich and baryon-free fluids with the weights of their energy densities in order to define a single quantity responsible for the vortical effects, in particular, the particle polarization. Thus, the proper-energy-density weighted kinematic vorticity is defined as

$$\Omega_{\mu\nu}(x, 0, z, t) = [\omega_{\mu\nu}^B(x, 0, z, t)\varepsilon_B(x, 0, z, t) + \omega_{\mu\nu}^f(x, 0, z, t)\varepsilon_f(x, 0, z, t)]/\langle\varepsilon(y=0, t)\rangle, \quad (6)$$

where ε_B and ε_f are the proper energy densities of the the baryon-rich and baryon-free fluids, respectively. The total proper energy density of all three fluids in the local rest frame, ε , is strictly defined as follows

$$\varepsilon = u_\mu T^{\mu\nu} u_\nu. \quad (7)$$

in terms of the total energy-momentum tensor $T^{\mu\nu} \equiv T_p^{\mu\nu} + T_t^{\mu\nu} + T_f^{\mu\nu}$ being the sum of conventional hydrodynamical energy-momentum tensors of separate fluids, and the total collective 4-velocity of the matter

$$u^\mu = u_\nu T^{\mu\nu} / (u_\lambda T^{\lambda\nu} u_\nu). \quad (8)$$

Note that definition (8) is, in fact, an equation determining u^μ . In general, this u^μ does not coincide with 4-velocities of separate fluids. However, in view of almost perfect unification of the baryon-rich fluids and small local baryon-fireball relative velocities, $v_{fB} \lesssim 0.2$, at $t \gtrsim 1$ fm/c, a very good approximation for ε is just

$$\varepsilon \simeq \varepsilon_B + \varepsilon_f. \quad (9)$$

The average energy density in the xz plane in Eq. (6) is

$$\langle\varepsilon(y, t)\rangle = \int dx dz \varepsilon(x, y, z, t) / \int_{\varepsilon(x, y, z, t) > 0} dx dz. \quad (10)$$

Similarly to $\Omega_{\mu\nu}$, we define the proper-energy-density weighted thermal vorticity in the reaction plane, though keep the same notation ($\varpi_{\mu\nu}$) for it.

The summation of $\omega_{\mu\nu}^B$ and $\omega_{\mu\nu}^f$ with the weights of their energy densities in Eq. (6) requires certain comments. Thus defined kinematic vorticity is very close to the true kinematic vorticity of the composed matter when the B- and f-velocities are close to each other. The latter is indeed the case at $t \gtrsim 1$ fm/c. Although, for the thermal vorticity this is not true. It is impossible to unambiguously define an effective temperature of the composed matter. Therefore, the energy-density-weighted sum for the thermal vorticity of a thermally non-equilibrated system is a certain ansatz giving us a possibility to analyze a nonequilibrium system in equilibrium terms. Nevertheless, this ansatz is very close to the true thermal vorticity in certain cases. As it was mentioned above, the f-fluid energy density is lower than that

of the unified baryon-rich fluid at $t > 4$ fm/c. Therefore, at $t > 4$ fm/c the f-fluid can be considered as small perturbation and hence this ansatz for the thermal vorticity of the composed matter is a good approximation.

The 3FD simulations of Au+Au collisions were performed without freeze-out. The freeze-out in the 3FD model removes the frozen out matter from the hydrodynamical evolution [30]. Therefore, in order to keep all the matter in the consideration the freeze-out was turned off.

Figure 2 presents the time evolution of the proper-energy-density weighted relativistic kinematic zx vorticity of the composed matter, see Eq. (6), the similarly weighted thermal zx vorticity, the QGP fraction, and the proper baryon and energy densities, Eqs. (2) and (7), respectively, in the reaction plain ($x\eta_s$) of central Au+Au collision at $\sqrt{s_{NN}} = 39$ GeV, where

$$\eta_s = \frac{1}{2} \ln \left(\frac{t+z}{t-z} \right) \quad (11)$$

is the longitudinal space-time rapidity and z is the coordinate along the beam direction. The advantage of this longitudinal space-time rapidity is that it is equal to the kinematic longitudinal rapidity defined in terms of the longitudinal velocity in the self-similar one-dimensional expansion of the system. As already mentioned, the baryon-rich fluids are mutually stopped and unified at $t \gtrsim 1$ fm/c. As the f-fluid is not that well unified with the combined baryon-rich fluid, the evolution of the f-fluid is separately presented in Fig. 3. The baryon-rich fluid entrains the f-fluid. This is the reason for the smallness of v_{fB} .

Thus, the dissipation in the system is very moderate at $t \gtrsim 1$ fm/c because the system is almost kinetically equilibrated. This smallness of the dissipation was confirmed by the analysis of the entropy production in the 3FD simulations [31]. Therefore, it may seem that an additional conservation law, i.e. the circulation conservation (Kelvin's circulation theorem), may be approximately valid. However, this is not the case. The Kelvin's circulation theorem was originally formulated for a so-called barotropic fluid, i.e. the fluid with the EoS of the type of $P = P(n_B)$, where P is the pressure. In fact, it is not important that P depends on n_B , it is important that P depends on a single variable (it can also be the energy density ε). In our case we have essentially $P = P(n_B, \varepsilon)$ because the system is essentially baryon-rich, as seen from Fig. 2. Therefore, the circulation is not conserved.

All major features of the collision dynamics are similar to those described in Ref. [27] for the central collision at the same energy. As seen from Fig. 2, at $t = 1$ fm/c the thermalized central (see the central bumps in n_B and ε) and primordial fragmentation regions, i.e. the baryon-rich matter passed through the interaction region (see two bumps of baryon density near $\eta_s = \pm 1$), have already been formed. The matter in all these regions is in the quark-gluon phase, see the QGP fraction in Fig. 2. There is a large fraction of the baryon charge stopped

in the central region. This is in contrast to the ultra-relativistic scenario (at the top RHIC and LHC energies) where the major part of the baryon charge is assumed to be located in the fragmentation regions already at the initial stage. The proper baryon and energy densities in this central region approximately are $n_B/n_0 \approx 10$ and $\varepsilon \approx 10$ GeV/fm³, respectively. The proper baryon density is similar to that attained in the central collision [27] while the energy one is considerably lower. The f-fluid dominates in this central energy density, as seen from Fig. 1.

In the course of time, the central region undergoes a rapid, practically self-similar one-dimensional (1D) expansion. In fact, the thermalized central region is produced in the state of this expansion. The matter, and in particular the baryon charge, is pushed out to the periphery of this central fireball, i.e. closer to the primordial fragmentation regions. The primordial fragmentation fireballs also expand in counter directions to the central one. The primordial fragmentation fireballs join with central contributions to the instant $t = 4$ fm/c because of their counter expansion, see Fig. 2. Therefore, the final fragmentation regions consist of primordial fragmentation fireballs and baryon-rich regions of the central fireball pushed out to peripheral rapidities. However, complete mixing of these central and primordial fragmentation fireballs does not occur, as seen from Fig. 3.

At later time $t \geq 8$ fm/c, see Figs. 2 and 3, the central part of the system gets frozen out while the fragmentation regions continue to evolve being already separated in the configuration space. This longer evolution of the fragmentation regions is due to the relativistic time dilation caused by their high-speed motion with respect to the central region. Therefore, their evolution time in the c.m. frame of colliding nuclei lasts ≈ 30 fm/c in the first-order-transition scenario and ≈ 25 fm/c in the crossover one.

From the very beginning the vortical fields, both the kinematic and thermal ones, are predominately formed at the periphery of the system, i.e. at the border between the participant and spectator matter, see Fig. 2. This means that the vorticity is initially located at peripheral rapidities rather than at midrapidity. Later on, the vortical fields partially spread to the participant and spectator bulk though remain concentrated near the border. In the conventional hydrodynamics this extension into the bulk is an effect of the shear viscosity. In the 3FD dynamics it is driven by the 3FD dissipation which imitates the effect of the shear viscosity [31]. The spread into the bulk, i.e. into the midrapidity region, is stronger at lower collision energies [11] because of the higher effective shear viscosity than that at higher energies [31]. This explains the drop of the vorticity value and consequently the observed hyperon polarization at the midrapidity with the collision energy rise.

At later times the maximum values in the vortical fields get more and more shifted to the fragmentation regions because of the 1D expansion of the system. At the same

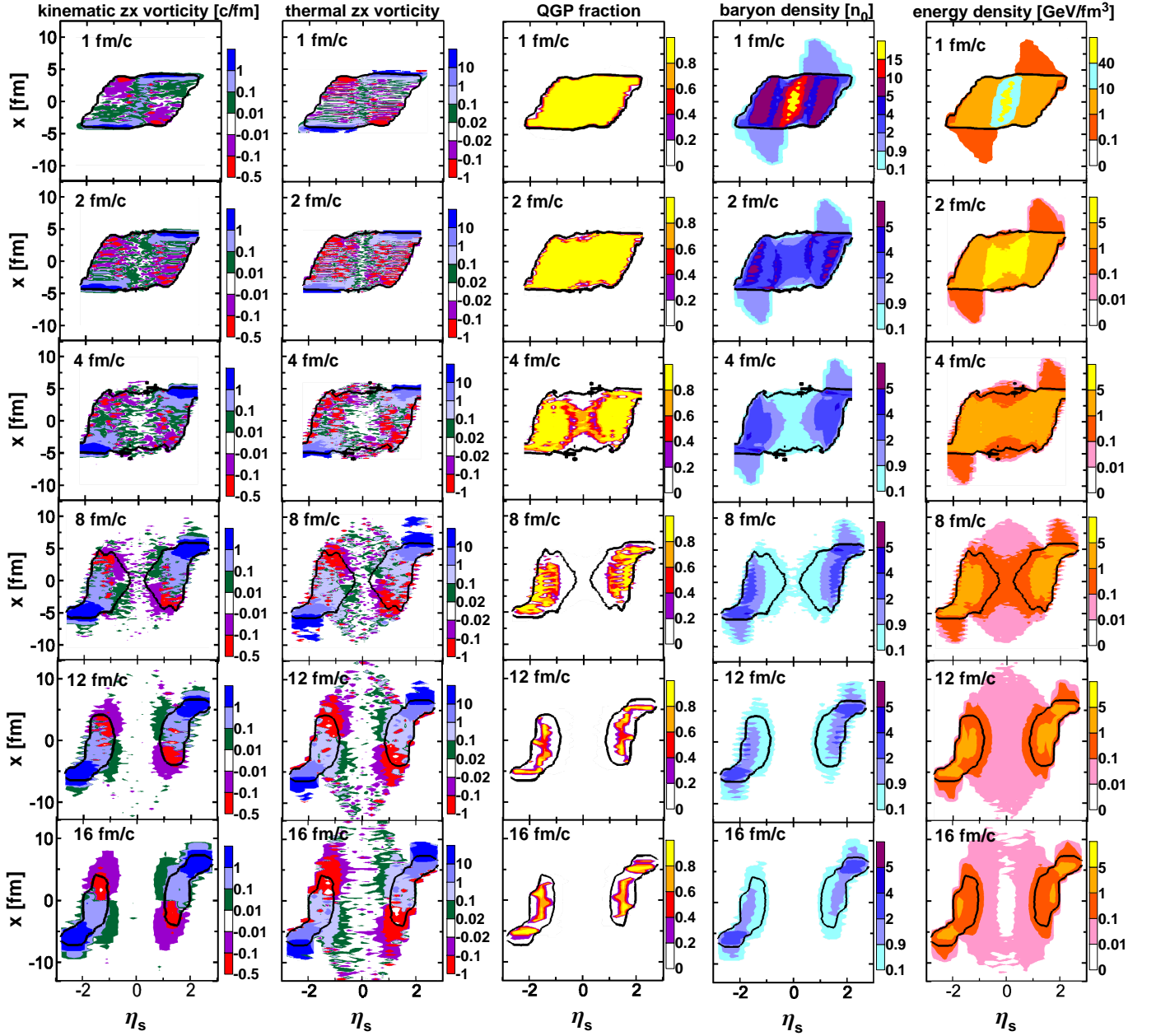


FIG. 2: (Color online) Columns from left to right: The proper-energy-density weighted relativistic kinematic zx vorticity, Eq. (6), the similarly weighted thermal zx vorticity, the QGP fraction, the proper baryon density (n_B) [see Eq. (2)] in units of the normal nuclear density ($n_0 = 0.15 \text{ 1/fm}^3$), and the proper energy density (ϵ), see Eq. (7), in the reaction plane at various time instants in the semi-central ($b = 6 \text{ fm}$) Au+Au collision at $\sqrt{s_{NN}} = 39 \text{ GeV}$. η_s is the space-time rapidity along the beam direction, see Eq. (11). Calculations are done with the first-order-phase-transition EoS. z axis is the beam direction. The bold solid contour displays the border of the frozen out matter. Inside this contour the matter still hydrodynamically evolves, while outside – it is frozen out.

time, the vorticity in the participant bulk gradually dissolves and practically disappears in the center of the colliding system. This longer evolution of the fragmentation regions is a result of the above mentioned relativistic time dilation caused by their high-speed motion with respect to the central region.

It is peculiarly that four strong oppositely directed vortices are formed at the periphery of the fragmentation

regions, see Fig. 2. These strong oppositely directed vortices predominantly consist of the baryon-rich matter because the f-fluid lags behind the primordial fragmentation matter, see Fig. 3. Over time, these vortices capture ever larger areas. The vortex at the border with the spectator matter is an order of magnitude stronger than its counterpart. This is the structure as it is seen in the reaction plane.

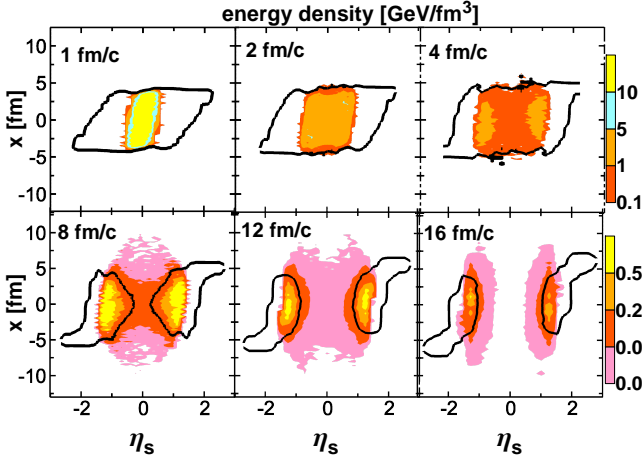


FIG. 3: (Color online) The proper energy density of the f-fluid in the reaction plane at various time instants in the semi-central ($b = 6$ fm) Au+Au collision at $\sqrt{s_{NN}} = 39$ GeV. η_s is the space-time rapidity along the beam direction. Calculations are done with the first-order-phase-transition EoS. z axis is the beam direction. The bold contours display the borders between the frozen-out and still hydrodynamically evolving matter.

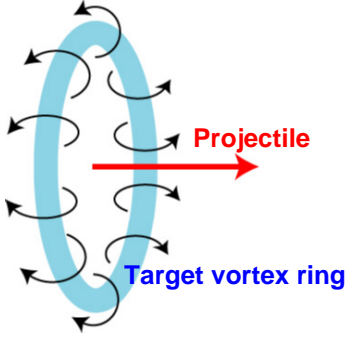


FIG. 4: (Color online) Schematic picture of the vortex ring in the target fragmentation region. Curled arrows indicate direction of the circulation of the target matter.

In fact, in three dimensions these are two vortex rings: one in the target fragmentation region and another in the projectile one. The matter rotation is opposite in this two rings. They are formed because the matter in the vicinity of the beam axis (z) is stronger decelerated because of thicker matter in the center than that at the periphery. Indeed, these rings are formed at the transverse periphery of the stopped matter in the central region, see the central bumps in n_B and ε at $t = 1$ fm/c in Fig. 2. Thus, the peripheral matter acquires a rotational motion. A schematic picture of the vortex ring in the target fragmentation region is presented in Fig. 4.

A similar effect was noticed in the analysis of the vorticity field [11–13] at energies of the Nuclotron-based Ion Collider fAcility (NICA) at the Joint Institute for Nuclear Research (JINR) in Dubna. The authors of Refs. [12, 13] called this specific toroidal structure as a femto-

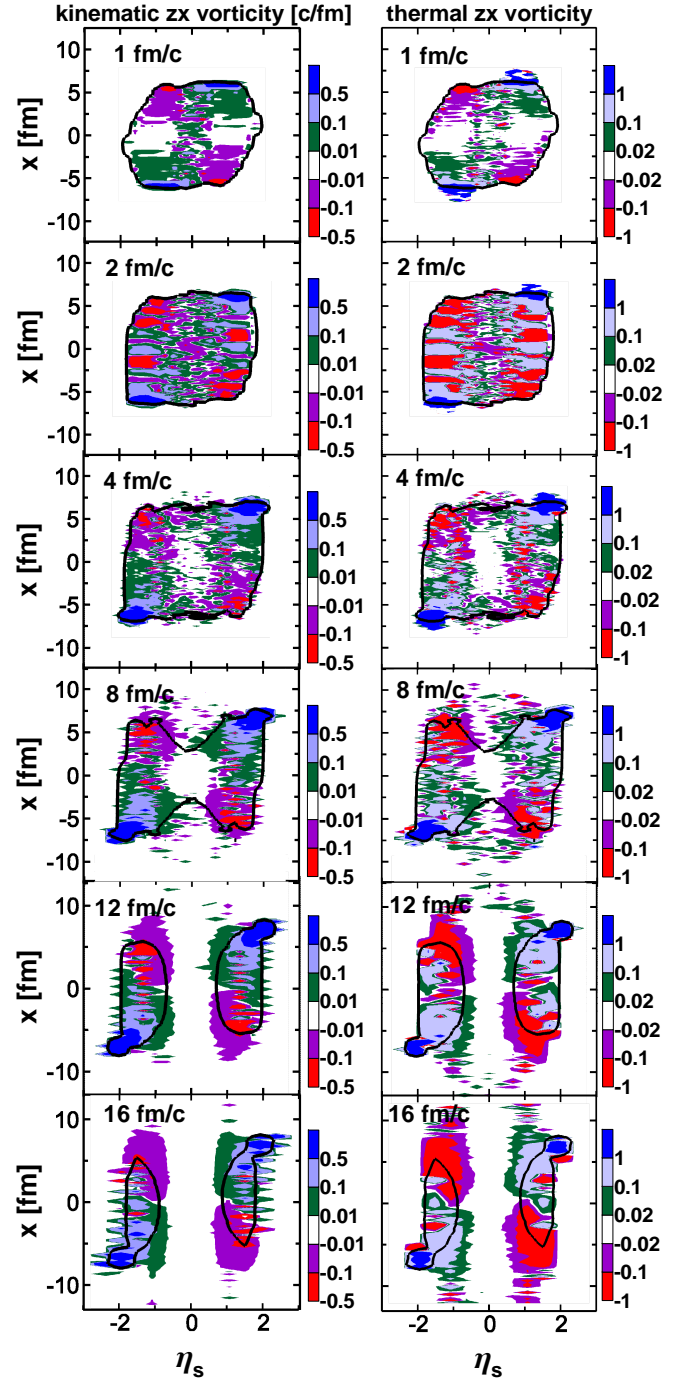


FIG. 5: (Color online) The same as in Fig. 2 but for the central ($b = 2$ fm) Au+Au collision at $\sqrt{s_{NN}} = 39$ GeV and without three right columns.

vortex sheet. This femto-vortex sheet is not a ring because the vorticity disappears in the xy plane, i.e. in the plane orthogonal to the reaction xz plane. At $\sqrt{s_{NN}} = 39$ GeV this femto-vortex sheet splits into two real rings, in which the vorticity does not disappear in the xy plane though is anisotropic in the x direction in noncentral collisions.

These rings are also formed in central collisions, as seen from Fig. 5. In the case of $b = 2$ fm the distribution of the vorticity along the rings is more homogeneous than that at $b = 6$ fm, but still the vorticity reaches high values. As seen from Fig. 5, the vortex rings are already formed at $t = 1$ fm/c with the vorticity predominantly concentrated at the periphery of the fragmentation zone. In the course of time the vorticity spreads into the bulk of the fragmentation regions. In fact, the schematic picture of the completely symmetric vortex ring, see Fig. 4, corresponds to the exactly central collision at $b = 0$.

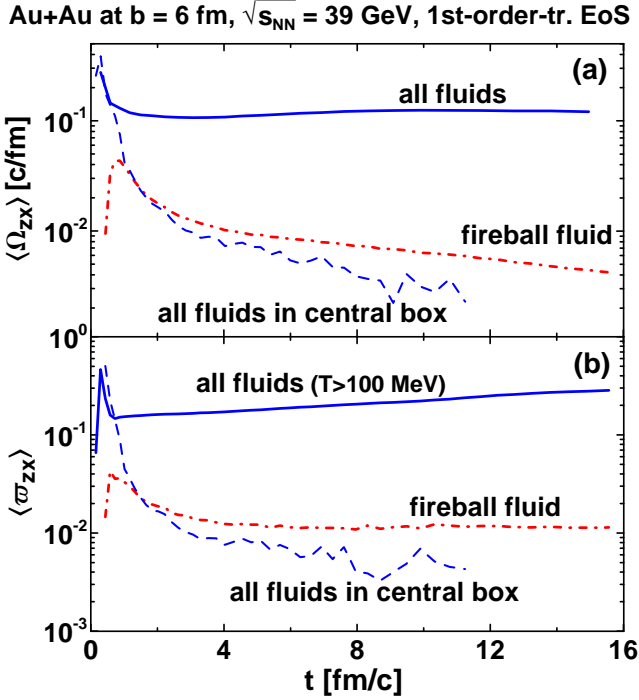


FIG. 6: (Color online) Time evolution of the proper-energy-weighted (a) relativistic kinematic zx vorticity and (b) thermal zx vorticity in the semi-central ($b = 6$ fm) Au+Au collision at $\sqrt{s_{NN}} = 39$ GeV. The vorticity of the composed matter, Eq. (12), and that of the f-fluid are averaged over the whole system. The thermal vorticity of the composed matter, Eq. (13), is averaged only over regions with high temperature, $T > 100$ MeV. The vorticities in the central box are averaged accordingly to Eqs. (12) and (13) but only over the central region $|x| < R - b/2$, $|y| < R - b/2$ and $|x| < R/\gamma_{cm}$, where R is the radius of the Au nucleus and γ_{cm} is the Lorentz factor associated with the initial nuclear motion in the c.m. frame. Calculations are done with the first-order-transition EoS.

In order to perform a more quantitative comparison of the vorticity in the midrapidity and fragmentation regions we calculated (kinematic and thermal) zx vorticity of the composed matter [in the sense of the ansatz of Eq. (6)] in the semi-central ($b = 6$ fm) Au+Au collision at $\sqrt{s_{NN}} = 39$ GeV averaged with the weight of the proper energy density over the whole system

$$\langle \Omega_{\mu\nu}(t) \rangle = \int dV [\omega_{\mu\nu}^B(\mathbf{x}, t) \varepsilon_B(\mathbf{x}, t)]$$

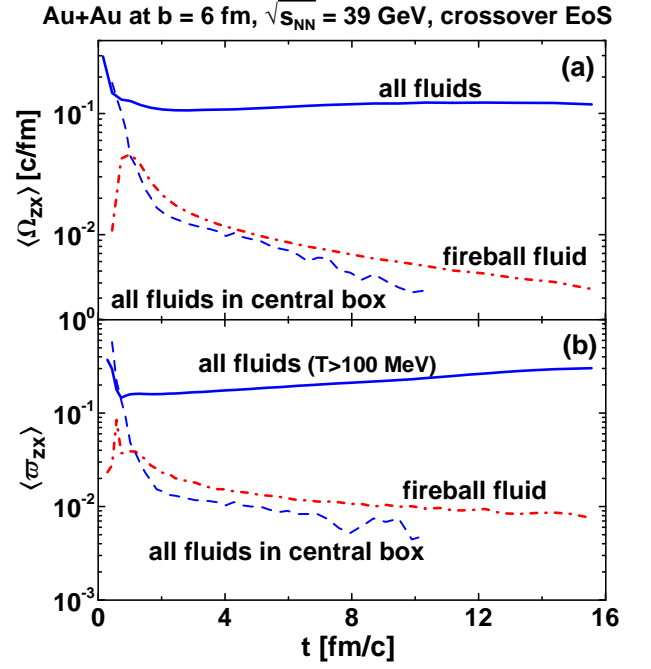


FIG. 7: (Color online) The same as in Fig. 6 but for the crossover EoS.

$$+ \omega_{\mu\nu}^f(\mathbf{x}, t) \varepsilon_f(\mathbf{x}, t)] / \langle \varepsilon(t) \rangle \quad (12)$$

$$\begin{aligned} \langle \varpi_{\mu\nu}(t) \rangle_{T>T_0} &= \int_{T>T_0} dV [\varpi_{\mu\nu}(\mathbf{x}, t) \varepsilon_B(\mathbf{x}, t) \\ &+ \varpi_{\mu\nu}^f(\mathbf{x}, t) \varepsilon_f(\mathbf{x}, t)] / \langle \varepsilon(t) \rangle_{T>T_0} \quad (13) \end{aligned}$$

where $T_0 = 100$ MeV is the temperature constraint. This temperature constraint is introduced because the temperature gradients and hence the thermal vorticity are very high at the spectator-participant border, where the temperature itself is not that high. At the same time, the Λ hyperons are abundantly produced from the hottest regions of the system. Therefore, we applied this temperature constraint on this averaging, keeping in mind application the Λ polarization. The average kinematic vorticity is not that strongly affected by the low-temperature contributions of the border regions [11]. This is why this constraint is omitted in the case of the kinematic vorticity.

The above average values of the vorticity are dominated by that in the fragmentation regions. Therefore, we use them as an estimates of the vorticity in the fragmentation regions, keeping in mind that the true vorticity in the fragmentation regions is even higher. To estimate the vorticity in the midrapidity region we perform averaging over only the center region of the system $|x| < R - b/2$, $|y| < R - b/2$ and $|x| < R/\gamma_{cm}$, where R is the radius of the Au nucleus and γ_{cm} is the Lorentz factor associated with the initial nuclear motion in the c.m. frame. In fact, this center region is a central layer because

it covers the whole participant region in the transverse direction.

Time evolution of the average relativistic kinematic and thermal zx vorticities calculated in the above described way is displayed in Figs. 6 and 7 for the two considered EoS's. The kinematic and thermal vorticities manifest very similar behavior. The vorticity of the f-fluid averaged with the ε_f weight over the whole system is separately presented. The f-fluid vorticity is more than an order of magnitude lower than that of the baryon-rich fluid, as it is expected from the negligible fraction of the total angular momentum accumulated in the f-fluid, see Fig. 1. The contribution of the f-fluid only slightly reduces the vorticity of the composed matter as compared with the baryon-rich vorticity at $t > 4$ fm/c, when the energy density of the f-fluid becomes small compared to the that of the baryon-rich fluid, see Fig. 1.

The average vorticity in the central region rapidly drops with time. At the early stage the average vorticity in the central region practically coincides with the total one since this central region includes practically the whole system because of the Lorentz contraction of colliding nuclei. Already at $t > 2$ fm/c, the central vorticity is more than an order of magnitude lower than the total one. It means the vorticity moves to the fragmentation regions.

The vorticity is redistributed in the process of the collision: the vorticity of the f-fluid drops, the vorticity moves from the central region to the fragmentation ones. Nevertheless, the average vorticity of the matter remains approximately constant in the process of the collision. The average thermal vorticity even slightly rises with time.

It is worthwhile to mention that the average vorticity displayed in Figs. 6 and 7 does not coincide with that of the frozen-out system. The freeze-out in the 3FD model is a continuous in time process [16, 30], as it is illustrated in Figs. 2 and 3. The actual vorticity of the frozen-out matter can be judged from the values of the vorticity field on the freeze-out contour in Figs. 2 and 3. As seen from Figs. 2 and 3, average values presented in Figs. 6 and 7 can be considered as order-of-magnitude estimates of the vorticity averaged over the frozen-out system at a fixed time instant.

IV. CONSEQUENCES FOR POLARIZATION

The above features of the vorticity imply certain consequences for the observable hyperon polarization. The vorticity cannot be presented as a function of the longitudinal rapidity because it is not an observable quantity. However, in the self-similar one-dimensional expansion of the system the longitudinal space-time rapidity (11) equals the kinematic longitudinal rapidity defined in terms of the longitudinal velocity. Thus, Fig. 2 gives an impression of the rapidity distribution of the vorticity and thereby the polarization. First of all, this distribution suggests that in semi-central collisions the polar-

ization in the fragmentation regions should be at least an order of magnitude higher than that observed by the STAR collaboration [4] in the midrapidity.

The global polarization results from asymmetry of the vortex rings which also asymmetrically expand in the transverse direction. The asymmetrical expansion results in directed flow of emitted particles. Hence, the global polarization in the fragmentation regions should be asymmetrical in the reaction plain with the Λ and $\bar{\Lambda}$ polarizations correlating with the corresponding directed flow.

In view of the strong global and even stronger local polarization expected in the fragmentation regions one comment is in order. The experimental observation of the global polarization [4] indicates that a strong spin-orbital coupling of some kind is present in the system. This coupling transfers the initially collective angular momentum into that accumulated in aligned spins of constituents of the system. If this part accumulated in the aligned spins is large, it should affect the collective dynamics of the system because the collective angular momentum is respectively reduced. This means the need to incorporate the medium polarization into the collective dynamics, e.g. the hydrodynamics [32, 33]. The present 3FD simulations were performed without such feedback.

V. SUMMARY

Within the 3FD model we have studied vorticity evolution in Au+Au collisions at $\sqrt{s_{NN}} = 39$ GeV. We considered two definitions of the vorticity—relativistic kinematic and thermal vorticities—that are relevant in different approaches to the hyperon polarization. As found, the kinematic and thermal vorticities manifest very similar behavior. Moreover, this behavior is very similar within the first-order-transition and crossover scenarios.

The vortical fields, both the kinematic and thermal ones, are predominately formed at the periphery of the system, i.e. at the border between the participant and spectator matter. This means that the vorticity is initially located at peripheral rapidities rather than at midrapidity. Later on, the vortical fields partially spread to the participant and spectator bulk though remain concentrated near the border.

A peculiar structure of two vortex rings is formed: one in the target fragmentation region and another in the projectile one. The matter rotation is opposite in this two rings. They are formed because the matter in the vicinity of the beam axis is stronger decelerated than that at the periphery because of thicker matter in the center. Thus, the peripheral matter acquires a rotational motion, which is inhomogeneous along the rings in noncentral collisions.

These rings are also formed in central collisions. In this case the distribution of the vorticity is more homogeneous than that in semi-central collisions, but still the vorticity reaches high values. These vortex rings are already formed at the early stage of the collision ($t = 1$

fm/c). The schematic picture of the completely symmetric vortex ring is presented in Fig. 4, corresponding to the exactly central collision.

The average vorticity is responsible for the global polarization of the observed Λ and $\bar{\Lambda}$ polarizations. In the semi-central collisions the average vorticity in the central region at $t > 2$ fm/c, when the central region can be associated with the midrapidity region, the central vorticity is more than an order of magnitude lower than the total one. The total vorticity is dominated contributions of the fragmentation regions and is produced because of the asymmetry of the above mentioned vortex rings.

The above features of the vorticity imply certain consequences for the observable hyperon polarization. First of all, they suggest that in semi-central collisions the global polarization in the fragmentation regions should be at least an order of magnitude higher than that observed by the STAR collaboration [4] in the midrapidity. This polarization should be asymmetrical in the reaction plain:

the Λ and $\bar{\Lambda}$ polarizations should correlate with the corresponding directed flow.

Acknowledgments

Fruitful discussions with D.N. Voskresensky are gratefully acknowledged. This work was carried out using computing resources of the federal collective usage center “Complex for simulation and data processing for mega-science facilities” at NRC “Kurchatov Institute”, <http://ckp.nrcki.ru/>. Y.B.I. was supported by the Russian Science Foundation, Grant No. 17-12-01427. A.A.S. was partially supported by the Ministry of Education and Science of the Russian Federation within the Academic Excellence Project of the NRNU MEPhI under contract No. 02.A03.21.0005.

-
- [1] Z. T. Liang and X. N. Wang, Phys. Rev. Lett. **94**, 102301 (2005) Erratum: [Phys. Rev. Lett. **96**, 039901 (2006)] doi:10.1103/PhysRevLett.94.102301, 10.1103/PhysRevLett.96.039901 [nucl-th/0410079].
 - [2] B. Betz, M. Gyulassy and G. Torrieri, Phys. Rev. C **76**, 044901 (2007) doi:10.1103/PhysRevC.76.044901 [arXiv:0708.0035 [nucl-th]].
 - [3] J. H. Gao, S. W. Chen, W. t. Deng, Z. T. Liang, Q. Wang and X. N. Wang, Phys. Rev. C **77**, 044902 (2008) doi:10.1103/PhysRevC.77.044902 [arXiv:0710.2943 [nucl-th]].
 - [4] L. Adamczyk *et al.* [STAR Collaboration], Nature **548**, 62 (2017) doi:10.1038/nature23004 [arXiv:1701.06657 [nucl-ex]].
 - [5] I. Karpenko and F. Becattini, Eur. Phys. J. C **77**, no. 4, 213 (2017) doi:10.1140/epjc/s10052-017-4765-1 [arXiv:1610.04717 [nucl-th]].
 - [6] Y. Xie, D. Wang and L. P. Csernai, Phys. Rev. C **95**, no. 3, 031901 (2017) doi:10.1103/PhysRevC.95.031901 [arXiv:1703.03770 [nucl-th]].
 - [7] M. Baznat, K. Gudima, A. Sorin and O. Teryaev, Phys. Rev. C **97**, no. 4, 041902 (2018) doi:10.1103/PhysRevC.97.041902 [arXiv:1701.00923 [nucl-th]]; M. Baznat, K. Gudima, G. Prokhorov, A. Sorin, O. Teryaev and V. Zakharov, J. Phys. Conf. Ser. **938**, no. 1, 012063 (2017). doi:10.1088/1742-6596/938/1/012063
 - [8] M. Baznat, K. Gudima, A. Sorin and O. Teryaev, EPJ Web Conf. **138**, 01008 (2017). doi:10.1051/epjconf/201713801008
 - [9] E. E. Kolomeitsev, V. D. Toneev and V. Voronyuk, arXiv:1801.07610 [nucl-th].
 - [10] H. Li, L. G. Pang, Q. Wang and X. L. Xia, Phys. Rev. C **96**, no. 5, 054908 (2017) doi:10.1103/PhysRevC.96.054908 [arXiv:1704.01507 [nucl-th]].
 - [11] Y. B. Ivanov and A. A. Soldatov, Phys. Rev. C **95**, no. 5, 054915 (2017) doi:10.1103/PhysRevC.95.054915 [arXiv:1701.01319 [nucl-th]].
 - [12] M. I. Baznat, K. K. Gudima, A. S. Sorin and O. V. Teryaev, Phys. Rev. C **93**, no. 3, 031902 (2016) doi:10.1103/PhysRevC.93.031902 [arXiv:1507.04652 [nucl-th]].
 - [13] M. Baznat, K. Gudima, A. Sorin and O. Teryaev, Phys. Rev. C **88**, no. 6, 061901 (2013) doi:10.1103/PhysRevC.88.061901 [arXiv:1301.7003 [nucl-th]].
 - [14] Y. Sun and C. M. Ko, Phys. Rev. C **96**, no. 2, 024906 (2017) doi:10.1103/PhysRevC.96.024906 [arXiv:1706.09467 [nucl-th]].
 - [15] S. J. Brodsky, F. Fleuret, C. Hadjidakis and J. P. Lansberg, Phys. Rept. **522**, 239 (2013) doi:10.1016/j.physrep.2012.10.001 [arXiv:1202.6585 [hep-ph]].
 - [16] Yu. B. Ivanov, V. N. Russkikh, and V.D. Toneev, Phys. Rev. C **73**, 044904 (2006) [nucl-th/0503088].
 - [17] Yu. B. Ivanov, Phys. Rev. C **87**, 064904 (2013) [arXiv:1302.5766 [nucl-th]].
 - [18] Y. B. Ivanov, Phys. Lett. B **721**, 123 (2013) doi:10.1016/j.physletb.2013.02.038 [arXiv:1211.2579 [hep-ph]]; Y. B. Ivanov and D. Blaschke, Phys. Rev. C **92**, no. 2, 024916 (2015) doi:10.1103/PhysRevC.92.024916 [arXiv:1504.03992 [nucl-th]].
 - [19] Y. B. Ivanov, Phys. Rev. C **87**, no. 6, 064905 (2013) doi:10.1103/PhysRevC.87.064905 [arXiv:1304.1638 [nucl-th]].
 - [20] Y. B. Ivanov, Phys. Rev. C **89**, no. 2, 024903 (2014) doi:10.1103/PhysRevC.89.024903 [arXiv:1311.0109 [nucl-th]].
 - [21] Y. B. Ivanov and A. A. Soldatov, Phys. Rev. C **91**, no. 2, 024914 (2015) doi:10.1103/PhysRevC.91.024914 [arXiv:1401.2265 [nucl-th]]; Y. B. Ivanov, Phys. Lett. B **723**, 475 (2013) doi:10.1016/j.physletb.2013.05.053 [arXiv:1304.2307 [nucl-th]].
 - [22] V. P. Konchakovski, W. Cassing, Y. B. Ivanov and V. D. Toneev, Phys. Rev. C **90**, no. 1, 014903 (2014) doi:10.1103/PhysRevC.90.014903 [arXiv:1404.2765 [nucl-th]]; Y. B. Ivanov and

- A. A. Soldatov, Phys. Rev. C **91**, no. 2, 024915 (2015) doi:10.1103/PhysRevC.91.024915 [arXiv:1412.1669 [nucl-th]]; Eur. Phys. J. A **52**, no. 1, 10 (2016) doi:10.1140/epja/i2016-16010-9 [arXiv:1601.03902 [nucl-th]].
- [23] Y. B. Ivanov and A. A. Soldatov, Phys. Rev. C **97**, no. 2, 024908 (2018) doi:10.1103/PhysRevC.97.024908 [arXiv:1801.01764 [nucl-th]].
- [24] L. Adamczyk *et al.* [STAR Collaboration], Phys. Rev. C **96**, no. 4, 044904 (2017) doi:10.1103/PhysRevC.96.044904 [arXiv:1701.07065 [nucl-ex]].
- [25] V. M. Galitsky and I. N. Mishustin, Sov. J. Nucl. Phys. **29**, 181 (1979).
- [26] A. S. Khvorostukhin, V. V. Skokov, K. Redlich, and V. D. Toneev, Eur. Phys. J. **C48**, 531 (2006) [nucl-th/0605069].
- [27] Y. B. Ivanov and A. A. Soldatov, Phys. Rev. C **97**, no. 2, 021901 (2018) doi:10.1103/PhysRevC.97.021901 [arXiv:1711.03069 [nucl-th]].
- [28] A. Sorin and O. Teryaev, Phys. Rev. C **95**, no. 1, 011902 (2017) doi:10.1103/PhysRevC.95.011902 [arXiv:1606.08398 [nucl-th]].
- [29] F. Becattini, V. Chandra, L. Del Zanna and E. Grossi, Annals Phys. **338**, 32 (2013) doi:10.1016/j.aop.2013.07.004 [arXiv:1303.3431 [nucl-th]].
- [30] V. N. Russkikh and Yu. B. Ivanov, Phys. Rev. C **76**, 054907 (2007) [nucl-th/0611094]; Yu. B. Ivanov and V. N. Russkikh, Phys. Atom. Nucl. **72**, 1238 (2009) [arXiv:0810.2262 [nucl-th]].
- [31] Y. B. Ivanov and A. A. Soldatov, Eur. Phys. J. A **52**, no. 5, 117 (2016) doi:10.1140/epja/i2016-16117-y [arXiv:1604.03261 [nucl-th]]; Eur. Phys. J. A **52**, no. 12, 367 (2016) doi:10.1140/epja/i2016-16367-7 [arXiv:1605.02476 [nucl-th]].
- [32] D. Montenegro, L. Tinti and G. Torrieri, Phys. Rev. D **96**, no. 5, 056012 (2017) Addendum: [Phys. Rev. D **96**, no. 7, 079901 (2017)] doi:10.1103/PhysRevD.96.079901, 10.1103/PhysRevD.96.056012 [arXiv:1701.08263 [hep-th]].
- [33] W. Florkowski, B. Friman, A. Jaiswal and E. Speranza, Phys. Rev. C **97**, no. 4, 041901 (2018) doi:10.1103/PhysRevC.97.041901 [arXiv:1705.00587 [nucl-th]].